

# Energy dependent kinetic freeze-out temperature and transverse flow velocity in high energy collisions

Li-Li Li, Fu-Hu Liu\*

*Institute of Theoretical Physics & State Key Laboratory of Quantum Optics and Quantum Optics Devices,  
Shanxi University, Taiyuan, Shanxi 030006, China*

**Abstract:** Transverse momentum spectra of negative and positive pions produced at mid-(pseudo)rapidity in inelastic or non-single-diffractive proton-proton collisions and in central nucleus-nucleus collisions over an energy range from a few GeV to above 10 TeV are analyzed by a (two-component) blast-wave model with Boltzmann-Gibbs statistics and with Tsallis statistics respectively. The model results are in similarly well agreement with the experimental data measured by a few productive collaborations who work at the Heavy Ion Synchrotron (SIS), Super Proton Synchrotron (SPS), Relativistic Heavy Ion Collider (RHIC), and Large Hadron Collider (LHC), respectively. The energy dependent kinetic freeze-out temperature and transverse flow velocity are obtained and analyzed. Both the quantities have quick increase from the SIS to SPS, and slight increase or approximate invariability from the top RHIC to LHC. Around the energy bridge from the SPS to RHIC, the considered quantities in proton-proton collisions obtained by the blast-wave model with Boltzmann-Gibbs statistics show more complex energy dependent behavior comparing with the results in other three cases.

**Keywords:** energy dependent kinetic freeze-out temperature, energy dependent transverse flow velocity, inelastic or non-single-diffractive proton-proton collisions, central nucleus-nucleus collisions

**PACS:** 12.40.Ee, 14.40.Aq, 24.10.Pa, 25.75.Ag

## 1 Introduction

The initial state, chemical freeze-out, and kinetic freeze-out are three main stages undergone by the interacting system in particle-particle, particle-nucleus, and nucleus-nucleus collisions at high energies. As the basic element (proton and neutron) in proton-nucleus and nucleus-nucleus collisions, proton-proton collisions display some similarities to proton-nucleus and nucleus-nucleus collisions. In particular, proton-proton collisions and gold-gold (copper-copper, lead-lead) collisions have been studying in large-scale experiments at the Heavy Ion Synchrotron (SIS), Super Proton Synchrotron (SPS), Relativistic Heavy Ion Collider (RHIC), and Large Hadron Collider (LHC). A few productive collaborations have been reporting abundant data on the particle ratios, (pseudo)rapidity spectra, transverse momentum (mass) spectra, invariant mass spectra, anisotropic flows, nuclear modification factor, and so on. Some useful information related to particle production and system evolution can be extracted from these data.

“Temperature is surely one of the central concepts in thermodynamics and statistical mechanics” [1]. The temperature in subatomic physics describes the excitation degree of the interacting system. Due to the system evolution, the temperature is expected to change at different stages. Undoubtedly, the kinetic freeze-out

temperature (the temperature at the kinetic freeze-out stage) is less than or equal to the chemical freeze-out temperature (the temperature at the chemical freeze-out stage) due to the fact that the kinetic freeze-out happens posteriorly or simultaneously comparing with the chemical freeze-out. The temperature at the initial state is the highest due to the largest compression and density during the process of system evolution. After the initial state, the interacting system undergoes transverse expansion and longitudinal extension. At the same time, some particles are emitted during the evolution process, though most particles are emitted at the kinetic freeze-out. The kinetic freeze-out temperature and concomitant transverse flow velocity can be extracted from the transverse momentum spectra of identified particles.

In order to extract the kinetic freeze-out temperature and transverse flow velocity and to study their dependence on energy, one can use different models to analyze the transverse momentum spectra. These models include, but are not limited to, the blast-wave model with Boltzmann-Gibbs statistics [2, 3] or with Tsallis statistics [4–6] and the alternative method [7–11] with standard distribution or with Tsallis distribution, where the standard distribution denotes the Boltzmann, Fermi-Dirac, and Bose-Einstein distributions. The blast-wave model can obtain simultaneously the kinetic freeze-out temperature and transverse flow velocity from single for-

\*E-mail: fuhuliu@163.com; fuhuliu@sxu.edu.cn

mula. The alternative method needs a few steps to obtain the two quantities, where the intercept in the linear relation of effective temperature against rest mass is regarded as the kinetic freeze-out temperature [7–11], and the slope in the linear relation of mean transverse momentum against mean moving mass (mean energy) is regarded as the transverse flow velocity [9–11]. The effective temperature is in fact the temperature parameter in the standard distribution in which the contribution of flow effect is not excluded. Comparatively, the blast-wave model is more convenient than the alternative method.

As we know, the energy dependent kinetic freeze-out temperature and transverse flow velocity in high energy collisions is an open question at present. We think that it is hard to conclude that whether or not there is an increase, decrease, or invariant trend with the increase of energy. In fact, the situations on the energy dependence of the kinetic freeze-out temperature and transverse flow velocity in literature are contradictory. Some of them show an increase trend [12–20], some of them show a decrease trend [15–20], and others show an invariant trend [12, 13] in the energy dependent kinetic freeze-out temperature and/or transverse flow velocity, with the increase of energy from the RHIC to LHC. Our recent work [21] shows an increase or invariant trend. As for the energy range from the SIS to SPS, the trend is always incremental in different literature. Indeed, It is necessary to do more studies on this topic and to conclude some affirmative conclusions.

In this paper, the blast-wave model with Boltzmann-Gibbs statistics [2, 3] and with Tsallis statistics [4] is used to extract the kinetic freeze-out temperature and transverse flow velocity by describing the transverse momentum spectra of negative and positive pions produced at mid-(pseudo)rapidity in inelastic (INEL) or non-single-diffractive (NSD) proton-proton ( $pp$  or  $p-p$ ) collisions and in central gold-gold (Au-Au) [copper-copper (Cu-Cu), lead-lead (Pb-Pb)] collisions over an energy range from the SIS to LHC. The model results are compared with the experimental data measured at the SIS, SPS, RHIC, and LHC by the FOPI [22], NA61/SHINE [23], PHENIX [24, 25], STAR [26–28], ALICE [29, 30], and CMS [31, 32] Collaborations. In some cases, two-component blast-wave model is used due to the fact that the single model can not fit the data very well.

This paper is structured as follows. The formalism and method are described in Section 2. Results and discussion are given in Section 3. In Section 4, we summarize our main observations and conclusions.

## 2 Formalism and method

Generally, the spectra in high transverse momentum region are contributed by the hard scattering process which is described by the quantum chromodynamics

(QCD) calculus [33–35] or the Hagedorn function [36, 37] which is in fact an inverse power law which has at least, in our opinion, three revisions. In refs. [38], [39–43], and [44], the three revisions of the Hagedorn function (inverse power law) are given respectively, though specific nomenclatures on the revised Hagedorn functions are not mentioned in some cases. We shall not discuss the Hagedorn function and its revisions due to the fact that the hard scattering process has no contribution to the kinetic freeze-out temperature and transverse flow velocity. Instead, the soft excitation process contributes the spectra in low transverse momentum region in which the kinetic freeze-out temperature and transverse flow velocity can be extracted.

In order to extract the kinetic freeze-out temperature and transverse flow velocity, we should analyze the spectra in low transverse momentum region. Although one can choose various functions to describe the mentioned spectra, the blast-wave model with Boltzmann-Gibbs statistics [2, 3] and with Tsallis statistics [4–6] is a convenient consideration. In particular, a single blast-wave model is not enough to describe the spectra in low transverse momentum region in some cases due to the contribution of resonance production or other reason such as statistical fluctuation. Then, a two-component blast-wave model is needed in these special cases.

According to refs. [2, 3], in the blast-wave model with Boltzmann-Gibbs statistics, the first component with the kinetic freeze-out temperature,  $T_1$ , and transverse flow velocity,  $\beta_{T1}$ , results in the probability density function of transverse momenta,  $p_T$ , to be

$$f(p_T, T_1, \beta_{T1}) = \frac{1}{N} \frac{dN}{dp_T} = C_1 p_T m_T \int_0^R r dr \times I_0 \left[ \frac{p_T \sinh(\rho_1)}{T_1} \right] K_1 \left[ \frac{m_T \cosh(\rho_1)}{T_1} \right], \quad (1)$$

where  $C_1$  is the normalized constant,  $m_T = \sqrt{p_T^2 + m_0^2}$  is the transverse mass,  $m_0$  is the rest mass,  $r/R$  is the relative radial position,  $I_0$  and  $K_1$  are the modified Bessel functions of the first and second kinds respectively,  $\rho_1 = \tanh^{-1}[\beta_1(r)]$  is the boost angle,  $\beta_1(r) = \beta_{S1}(r/R)^{n_0}$  is a self-similar flow profile,  $\beta_{S1}$  is the flow velocity on the surface, and  $n_0 = 2$  is used in the original form [2]. As a mean of  $\beta_1(r)$ ,  $\beta_{T1} = (2/R^2) \int_0^R r \beta_1(r) dr = 2\beta_{S1}/(n_0 + 2)$ .

According to ref. [4–6], in the blast-wave model with Tsallis statistics, the first component with  $T_1$  and  $\beta_{T1}$  results in the probability density function of  $p_T$  to be

$$f(p_T, T_1, \beta_{T1}) = \frac{1}{N} \frac{dN}{dp_T} = C_1 p_T m_T \int_{-\pi}^{\pi} d\phi \int_0^R r dr \times \left\{ 1 + \frac{q-1}{T_0} [m_T \cosh(\rho) - p_T \sinh(\rho) \cos(\phi)] \right\}^{-1/(q-1)}, \quad (2)$$

where  $q$  is an entropy index that characterizes the degree of non-equilibrium,  $\phi$  denotes the azimuthal angle, and  $n_0 = 1$  is used in the original form [4]. It should be noted that  $f(p_T, T_1, \beta_{T1})$ ,  $T_1$ ,  $\beta_{T1}$ , and  $C_1$  in Eq. (2) are different from those in Eq. (1), though the same symbols are used.

The second component has the same form as the first one, but with the kinetic freeze-out temperature,  $T_2$ , and transverse flow velocity,  $\beta_{T2}$ . The two-component blast-wave model can be structured as

$$f_0(p_T) = \frac{1}{N} \frac{dN}{dp_T} = kf(p_T, T_1, \beta_{T1}) + (1 - k)f(p_T, T_2, \beta_{T2}), \quad (3)$$

where  $k$  denotes the contribution fraction (rate) of the first component.

According to Hagedorn's model [36], we may also use the usual step function to structure the two-component blast-wave model. That is

$$f_0(p_T) = \frac{1}{N} \frac{dN}{dp_T} = A_1 \theta(p_1 - p_T) f(p_T, T_1, \beta_{T1}) + A_2 \theta(p_T - p_1) f(p_T, T_2, \beta_{T2}), \quad (4)$$

where  $A_1$  and  $A_2$  are constants which result in the two components to be equal to each other at  $p_T = p_1$ ,  $\theta(p_1 - p_T) = 1$  (or 0) if  $p_T < p_1$  (or  $p_T > p_1$ ), and  $\theta(p_T - p_1) = 1$  (or 0) if  $p_T > p_1$  (or  $p_T < p_1$ ).

Both Eqs. (3) and (4) can be used to extract the kinetic freeze-out temperature,  $T_0$ , and transverse flow velocity,  $\beta_T$ , in the two-component blast-wave model. We have

$$T_0 = kT_1 + (1 - k)T_2 \quad (5)$$

and

$$\beta_T = k\beta_{T1} + (1 - k)\beta_{T2}. \quad (6)$$

In the case of using Eq. (3) to get the parameter values of two components,  $k$  is directly given by Eq. (3). In the case of using Eq. (4) to get the parameter values of two components,  $k$  is expressed by

$$k = \int_0^{p_1} A_1 f(p_T, T_1, \beta_{T1}) dp_T \quad (7)$$

due to Eq. (4) is the probability density function which results naturally in the normalization.

There are little difference between values of  $T_0$  ( $\beta_T$ ) extracted from Eqs. (3) and (4). Generally,  $T_1$  ( $\beta_{T1}$ ) from Eq. (3) is less than that from Eq. (4) by  $\leq 5\%$ , and  $T_2$  ( $\beta_{T2}$ ) from Eq. (3) is larger than that from Eq. (4) by  $\leq 5\%$ . As a combination of the two components,  $T_0$  ( $\beta_T$ ) from Eq. (3) is less than that from Eq. (4) by  $< 5\%$  due to the dominant role of the first component.

We are inclined to use Eq. (3) due to its convenient fit in obtaining a smooth curve, though there is decussate region between the contributions of the two components in Eq. (3). Oppositely, Eq. (4) is hard to get a smooth curve at  $p_T = p_1$ , though there is no entanglement between the two components in Eq. (4).

To describe the system and statistics clearly, we divide the subject investigated in the present work into four cases. The case I is the case which describes  $pp$  collisions by the blast-wave model with Boltzmann-Gibbs statistics. The case II is the case which describes  $pp$  collisions by the blast-wave model with Tsallis statistics. The case III is the case which describes nucleus-nucleus collisions by the blast-wave model with Boltzmann-Gibbs statistics. And the case IV is the case which describes nucleus-nucleus collisions by the blast-wave model with Tsallis statistics.

### 3 Results and discussion

The transverse momentum spectra of  $\pi^-$  and  $\pi^+$  produced at mid-(pseudo)rapidity in INEL or NSD  $pp$  collisions at high energies are presented in Fig.1, where different mid-(pseudo)rapidity ( $y$  or  $\eta$ ) intervals and collision energies ( $\sqrt{s}$ ) are marked in the panels. The closed (open) symbols presented in panels (a)–(e) represent the data of  $\pi^-$  ( $\pi^+$ ) measured by the NA61/SHINE [23], PHENIX [24], STAR [26], ALICE [29], and CMS [31, 32] Collaborations, respectively, where in panel (a) only the spectra of  $\pi^-$  are available, and panel (c) is for NSD events and other panels are for INEL events. The solid (dashed) curves are our results calculated by Eqs. (1) and (3) for  $\pi^-$  ( $\pi^+$ ) (case I), and the dotted (dotted-dashed) curves are our results calculated by Eqs. (2) and (3) for  $\pi^-$  ( $\pi^+$ ) (case II). Different forms of the spectra are used due to different Collaborations, where  $N$ ,  $E$ ,  $p$ ,  $\sigma$ , and  $N_{EV}$  denote the particle number, energy, momentum, cross-section, and event number, respectively. In some cases, different amounts marked in the panels are used to scale the data for clarity. The continuous panels (a)–(e) shows the ratios of data to fit obtained from Eqs. (1) and (3) for the case I, corresponding to the collisions shown in the  $p_T$  spectra; and the continuous panels (a')–(e') shows the ratios of data to fit obtained from Eqs. (2) and (3) for the case II. The values of free parameters ( $T_1$ ,  $T_2$ ,  $\beta_{T1}$ ,  $\beta_{T2}$ , and  $k$ , as well as  $q$  if available), derived parameters ( $T_0$  and  $\beta_T$ ), normalization constant ( $N_0$ ),  $\chi^2$ , and degrees of freedom (dof) corresponding to the curves in Fig. 1 are listed in Tables 1 and 2 for the cases I and II respectively. One can see that Eq. (3) describes similarly well the  $p_T$  spectra at mid-(pseudo)rapidity in INEL or NSD  $pp$  collisions over an energy range from a few GeV to above 10 TeV. The main parameters ( $T_0$  and  $\beta_T$ ) show some laws in the considered energy range, which will be discussed later.

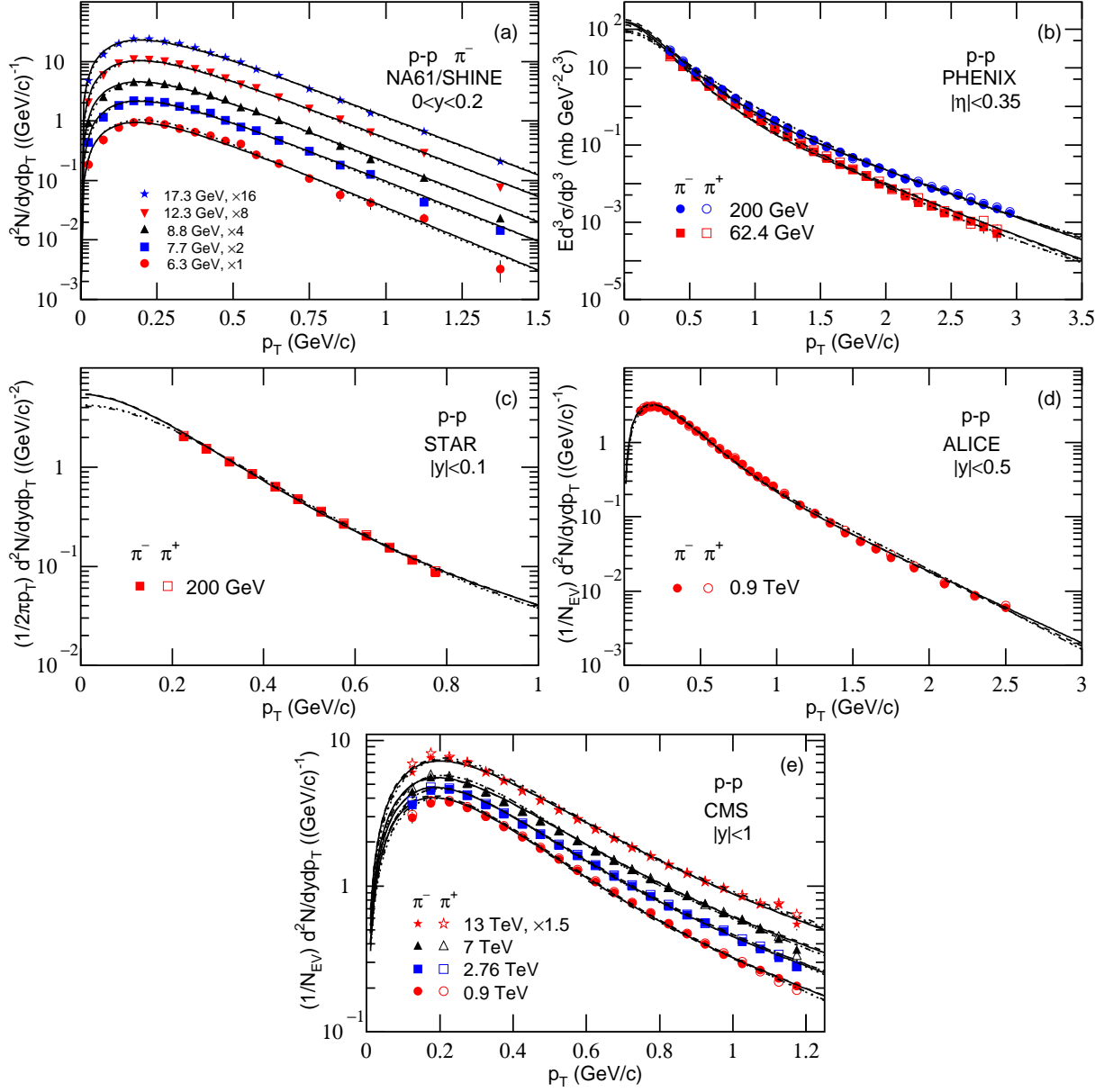


Fig. 1. Transverse momentum spectra of  $\pi^-$  and  $\pi^+$  produced at mid-(pseudo)rapidity in INEL or NSD  $pp$  collisions at high energies, where the mid-(pseudo)rapidity intervals and energies are marked in the panels. Panels (a)–(e) represent the data measured by the NA61/SHINE [23], PHENIX [24], STAR [26], ALICE [29], and CMS [31, 32] Collaborations, respectively, by various symbols, where in panel (a) only the spectra of  $\pi^-$  are available, and panel (c) is for NSD events and other panels are for INEL events. In some cases, different amounts marked in the panels are used to scale the data for clarity. The solid (dashed) curves are our results calculated by Eqs. (1) and (3) for  $\pi^-$  ( $\pi^+$ ) (case I), and the dotted (dotted-dashed) curves are our results calculated by Eqs. (2) and (3) for  $\pi^-$  ( $\pi^+$ ) (case II). Continuous panels (a)–(e) and (a')–(e') are for ratios of the data to fit obtained from Eqs. (1) and (3) for the case I and from Eqs. (2) and (3) for the case II respectively, corresponding to the collisions shown in the  $p_T$  spectra.

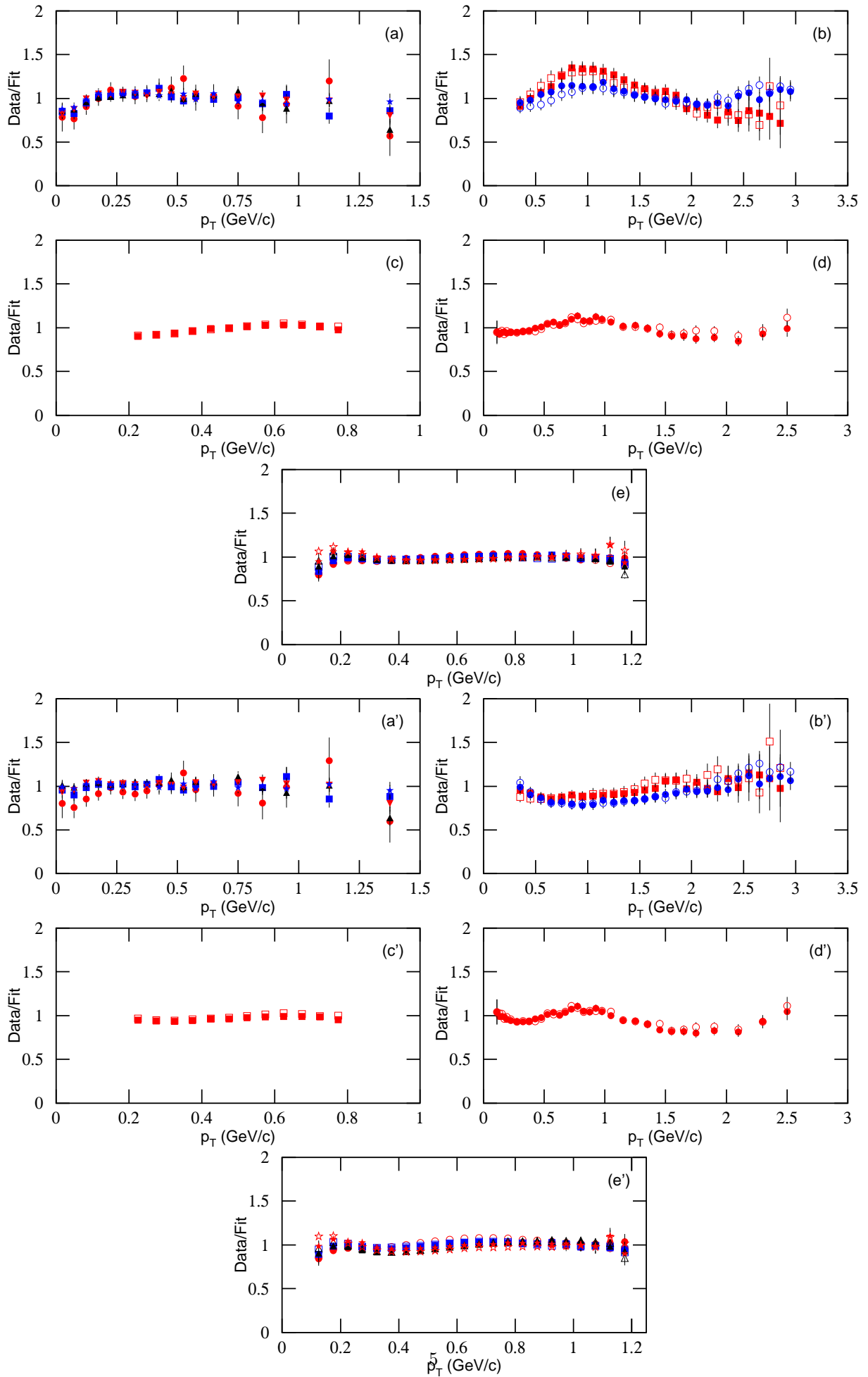


Fig. 1. Continuous.

Figure 2 is the same as Fig. 1, but it shows the results at mid-rapidity in central Au-Au (Cu-Cu, Pb-Pb) collisions at high energies. The symbols in panels (a)–(f) represent the data measured by the FOPI [22], STAR [27], STAR [28], PHENIX [25], STAR [26], and ALICE [30] Collaborations, respectively, with different mid-rapidity intervals, centrality intervals, and collision energies. The solid (dashed) curves are our results calculated by Eqs. (1) and (3) for  $\pi^-$  ( $\pi^+$ ) (case III), and the dotted (dotted-dashed) curves are our results calculated by Eqs. (2) and (3) for  $\pi^-$  ( $\pi^+$ ) (case IV). The continuous panels (a)–(f) and (a')–(f') show the ratios of data to fit. The values of various parameters,  $\chi^2$ , and dof corresponding to the curves in Fig. 2 are listed in Tables 3 and 4 for the cases III and IV respectively. One can see that Eqs. (2) and (3) describe similarly well the  $p_T$  spectra at mid-(pseudo)rapidity in central Au-Au (Cu-Cu, Pb-Pb) collisions at different energies per nucleon pair ( $\sqrt{s_{NN}}$ ) in center-of-mass system.

The energy dependent  $T_0$  and  $\beta_T$  are presented in the upper and lower panels in Fig. 3 respectively, where the left and right panels correspond to the results obtained from Eqs. (1) and (3) and from Eqs. (2) and (3) respectively. The closed and open symbols represent the parameter values corresponding to  $\pi^-$  and  $\pi^+$  respectively, which are listed in Tables 1 and 2 for the cases I and II respectively, for INEL or NSD  $pp$  collisions, and in Tables 3 and 4 for the cases III and IV respectively, for central Au-Au (Cu-Cu, Pb-Pb) collisions. One can see that the difference between the results of  $\pi^-$  and  $\pi^+$  can be neglected. In the energy dependent  $T_0$  and  $\beta_T$  in INEL or NSD  $pp$  collisions obtained by the blast-wave model with Boltzmann-Gibbs statistics (case I), there are a hill at  $\sqrt{s} \approx 10$  GeV, a drop at dozens of GeV, and then an increase from dozens of GeV to above 10 TeV. The energy dependent  $T_0$  and  $\beta_T$  in other three cases show a simple structure. That is, there is a quick increase from the SIS to SPS. Then, a slight increase or similar invariability appears from the RHIC to LHC. Special structure is not observed around the energy bridge from the SPS to RHIC in other three cases, though lower  $T_0$  and  $\beta_T$  are obtained in the cases II and IV in which the Tsallis statistics is used.

It should be noted that the fit of the first two points in Fig. 1(a) is extortionate in some cases. It means  $T_0$  ( $\beta_T$ ) for  $pp$  collisions at the SPS could be higher than that what is shown in Fig. 3 in the case of improving the fit. Contrarily, the fit of the first point in Fig. 2(d) is too low. It means  $T_0$  ( $\beta_T$ ) for central Cu-Cu collisions at 22.5 GeV could be lower than that what is shown in Fig. 3. We give up to improve further the fit of the first one or two points due to the trend of whole fit being worse. Alternatively, we may use a multi-component model to improve further the fit. The changed amounts in  $T_0$  ( $\beta_T$ ) caused by the further improvement are small.

Since  $T_0$  ( $\beta_T$ ) is strongly related to mean transverse momentum,  $\langle p_T \rangle$ , or root-mean-square transverse mo-

mentum,  $\sqrt{\langle p_T^2 \rangle}$ , we plot  $\langle p_T \rangle$  against  $\sqrt{s}$  ( $\sqrt{s_{NN}}$ ) and  $\sqrt{\langle p_T^2 \rangle}$  against  $\sqrt{s}$  ( $\sqrt{s_{NN}}$ ) in the upper and lower panels in Fig. 4 respectively, to check if the discontinuous hill in the case I still exists, where the left and right panels correspond to the results obtained from Eqs. (1) and (3) and from Eqs. (2) and (3) respectively. One can see that the hill in Fig. 3 is obviously smoothed in Fig. 4 for the case I. Similar trend as what is shown in Fig. 3 is observed in Fig. 4 for other three cases.

It should be noted that the above calculations in Fig. 4 are done according to the functions of curves in the  $p_T$  range from 0 to 5 GeV/c, though the experimental  $p_T$  ranges are different and much shorter. If we reduce the  $p_T$  range, the trend does not change obviously due to small fraction of particles with high  $p_T$ . We give up to use the experimental data to calculate  $\langle p_T \rangle$  and  $\sqrt{\langle p_T^2 \rangle}$  due to the fact that some data are incomplete in the considered  $p_T$  range, in particular in very-low- $p_T$  region.

Comparing with the case I, the different situation of energy dependence of  $T_0$  ( $\beta_T$ ) in other three cases is caused by larger collision systems for central nucleus-nucleus collisions and/or one more parameter ( $q$ ) in the Tsallis statistics. In central nucleus-nucleus collisions, some statistical and/or dynamical fluctuations existed in small collision systems are smoothed because of the successional or cascade nucleon-nucleon collisions and the multiple scattering of secondary particles. In the Tsallis statistics, some fluctuations existed in two-component Boltzmann-Gibbs statistics are smoothed due to the introduction of  $q$  which causes more entanglements in the selections of  $T_0$  and  $\beta_T$ . These factors cause the energy dependent  $T_0$  ( $\beta_T$ ) in other three cases is different from that in the case I.

In any case, the special structure around 10 GeV in the energy dependent  $T_0$  ( $\beta_T$ ) in the case I or the different trend which turns a corner in other three cases indicates that this energy is special as pointed out by Cleymans [45]. The present work shows that, in most cases, the energy dependent  $T_0$  ( $\beta_T$ ) increases quickly before 10 GeV and then saturates or increases slowly after 10 GeV with the increase of collision energy, which also indicates this special energy (11 GeV more specifically [45]). Some special properties result in this special energy. The final state has the highest net baryon density at this energy. Meanwhile, there is a transition from a baryon-dominated to a meson-dominated final state, and the ratios of strange particles to mesons show clear and pronounced maximums [45].

At 11 GeV, the chemical freeze-out temperature in central nucleus-nucleus collisions is  $T_{ch} \approx 151$  MeV [45]. The present work shows that, at this energy, the kinetic freeze-out temperature in INEL or NSD  $pp$  collisions is  $T_0 \approx 115$  MeV and that in central nucleus-nucleus collisions is  $T_0 \approx 125$  MeV, obtained from Eqs. (1) and (3). The differences between  $T_{ch}$  and  $T_0$  and be-

Table 1. Values of free parameters ( $T_1$ ,  $T_2$ ,  $\beta_{T1}$ ,  $\beta_{T2}$ , and  $k$ ), normalization constant ( $N_0$ ), and  $\chi^2/\text{dof}$  corresponding to the solid and dashed curves in Fig. 1 in which different data are measured in different mid-(pseudo)rapidity intervals at different energies by different Collaborations. The derived parameters  $T = kT_1 + (1 - k)T_2$  and  $\beta_T = k\beta_{T1} + (1 - k)\beta_{T2}$ .

Collab.	$\sqrt{s}$ (GeV)	Particle	$T_1$ (MeV)	$T_2$ (MeV)	$T$ (MeV)	$k$	$\beta_{T1}$ (c)	$\beta_{T2}$ (c)	$\beta_T$ (c)	$N_0$	$\chi^2/\text{dof}$
NA61/SHINE	6.3	$\pi^-$	$110 \pm 6$	—	$110 \pm 6$	1	$0.36 \pm 0.02$	—	$0.36 \pm 0.02$	$0.08 \pm 0.01$	19/15
	7.7	$\pi^-$	$114 \pm 6$	—	$114 \pm 6$	1	$0.36 \pm 0.02$	—	$0.36 \pm 0.02$	$0.10 \pm 0.01$	25/15
	8.8	$\pi^-$	$114 \pm 6$	—	$114 \pm 6$	1	$0.36 \pm 0.02$	—	$0.36 \pm 0.02$	$0.10 \pm 0.01$	48/15
	12.3	$\pi^-$	$117 \pm 6$	—	$117 \pm 6$	1	$0.37 \pm 0.02$	—	$0.37 \pm 0.02$	$0.12 \pm 0.01$	34/15
	17.3	$\pi^+$	$117 \pm 6$	—	$117 \pm 6$	1	$0.37 \pm 0.02$	—	$0.37 \pm 0.02$	$0.13 \pm 0.01$	15/15
PHENIX	62.4	$\pi^-$	$96 \pm 5$	$203 \pm 10$	$97 \pm 5$	$0.99 \pm 0.01$	$0.27 \pm 0.01$	$0.37 \pm 0.02$	$0.27 \pm 0.01$	$23.04 \pm 1.15$	137/20
		$\pi^+$	$96 \pm 5$	$224 \pm 11$	$98 \pm 5$	$0.99 \pm 0.01$	$0.27 \pm 0.01$	$0.28 \pm 0.01$	$0.27 \pm 0.01$	$20.81 \pm 1.04$	83/20
	200	$\pi^-$	$101 \pm 5$	$238 \pm 12$	$102 \pm 5$	$0.99 \pm 0.01$	$0.29 \pm 0.02$	$0.32 \pm 0.02$	$0.29 \pm 0.01$	$27.69 \pm 1.38$	28/21
		$\pi^+$	$101 \pm 5$	$229 \pm 12$	$102 \pm 5$	$0.99 \pm 0.01$	$0.29 \pm 0.02$	$0.36 \pm 0.02$	$0.29 \pm 0.01$	$31.14 \pm 1.56$	28/21
STAR	200	$\pi^-$	$103 \pm 5$	$222 \pm 14$	$105 \pm 5$	$0.98 \pm 0.01$	$0.29 \pm 0.02$	$0.35 \pm 0.02$	$0.30 \pm 0.01$	$0.29 \pm 0.01$	75/6
		$\pi^+$	$103 \pm 5$	$225 \pm 15$	$105 \pm 5$	$0.98 \pm 0.01$	$0.29 \pm 0.02$	$0.35 \pm 0.02$	$0.30 \pm 0.01$	$0.29 \pm 0.01$	90/6
ALICE	900	$\pi^-$	$104 \pm 5$	$257 \pm 13$	$106 \pm 5$	$0.99 \pm 0.01$	$0.31 \pm 0.02$	$0.33 \pm 0.02$	$0.31 \pm 0.02$	$1.51 \pm 0.08$	120/27
		$\pi^+$	$104 \pm 5$	$259 \pm 13$	$106 \pm 5$	$0.99 \pm 0.01$	$0.31 \pm 0.02$	$0.30 \pm 0.02$	$0.31 \pm 0.02$	$1.52 \pm 0.08$	93/27
CMS	900	$\pi^-$	$103 \pm 5$	$272 \pm 14$	$105 \pm 5$	$0.99 \pm 0.01$	$0.32 \pm 0.02$	$0.39 \pm 0.02$	$0.32 \pm 0.02$	$3.82 \pm 0.19$	41/16
		$\pi^+$	$103 \pm 5$	$270 \pm 14$	$105 \pm 5$	$0.99 \pm 0.01$	$0.31 \pm 0.02$	$0.39 \pm 0.02$	$0.31 \pm 0.02$	$3.92 \pm 0.20$	46/16
	2760	$\pi^-$	$106 \pm 5$	$281 \pm 14$	$109 \pm 5$	$0.99 \pm 0.01$	$0.33 \pm 0.02$	$0.41 \pm 0.02$	$0.33 \pm 0.02$	$4.71 \pm 0.24$	26/16
		$\pi^+$	$106 \pm 5$	$289 \pm 14$	$109 \pm 5$	$0.99 \pm 0.01$	$0.33 \pm 0.02$	$0.36 \pm 0.02$	$0.33 \pm 0.02$	$4.76 \pm 0.24$	17/16
	7000	$\pi^-$	$109 \pm 5$	$296 \pm 15$	$112 \pm 5$	$0.99 \pm 0.01$	$0.36 \pm 0.02$	$0.40 \pm 0.02$	$0.36 \pm 0.02$	$5.77 \pm 0.29$	34/16
		$\pi^+$	$109 \pm 5$	$296 \pm 15$	$112 \pm 5$	$0.99 \pm 0.01$	$0.37 \pm 0.02$	$0.43 \pm 0.02$	$0.37 \pm 0.02$	$5.75 \pm 0.29$	36/16
	1300	$\pi^-$	$112 \pm 6$	$288 \pm 14$	$114 \pm 6$	$0.99 \pm 0.01$	$0.40 \pm 0.02$	$0.49 \pm 0.02$	$0.40 \pm 0.02$	$5.20 \pm 0.26$	18/16
		$\pi^+$	$111 \pm 6$	$293 \pm 15$	$114 \pm 6$	$0.99 \pm 0.01$	$0.40 \pm 0.02$	$0.49 \pm 0.02$	$0.40 \pm 0.02$	$5.27 \pm 0.26$	26/16

Table 2. Same as Table 1, but one more parameter ( $q$ ) is added and the values correspond to the dotted and dotted-dashed curves in Fig. 1.

Collab.	$\sqrt{s}$ (GeV)	Particle	$T_1$ (MeV)	$T_2$ (MeV)	$T$ (MeV)	$k$	$\beta_{T1}$ (c)	$\beta_{T2}$ (c)	$\beta_T$ (c)	$q$	$N_0$	$\chi^2/\text{dof}$
NA61/SHINE	6.3	$\pi^-$	$80 \pm 4$	—	$80 \pm 4$	1	$0.18 \pm 0.01$	—	$0.18 \pm 0.01$	$1.052 \pm 0.009$	$0.08 \pm 0.01$	19/15
	7.7	$\pi^-$	$83 \pm 4$	—	$83 \pm 4$	1	$0.21 \pm 0.01$	—	$0.21 \pm 0.01$	$1.053 \pm 0.009$	$0.10 \pm 0.01$	9/15
	8.8	$\pi^-$	$84 \pm 5$	—	$84 \pm 5$	1	$0.21 \pm 0.01$	—	$0.21 \pm 0.01$	$1.053 \pm 0.008$	$0.10 \pm 0.01$	29/15
	12.3	$\pi^-$	$84 \pm 5$	—	$84 \pm 5$	1	$0.21 \pm 0.01$	—	$0.21 \pm 0.01$	$1.055 \pm 0.008$	$0.12 \pm 0.01$	13/15
	17.3	$\pi^+$	$85 \pm 4$	—	$85 \pm 4$	1	$0.21 \pm 0.01$	—	$0.21 \pm 0.01$	$1.056 \pm 0.007$	$0.13 \pm 0.01$	3/15
PHENIX	62.4	$\pi^-$	$80 \pm 4$	—	$80 \pm 4$	1	$0.21 \pm 0.01$	—	$0.21 \pm 0.01$	$1.074 \pm 0.008$	$20.36 \pm 1.02$	47/20
		$\pi^+$	$80 \pm 4$	—	$80 \pm 4$	1	$0.21 \pm 0.01$	—	$0.21 \pm 0.01$	$1.074 \pm 0.008$	$20.94 \pm 1.05$	49/20
	200	$\pi^-$	$81 \pm 4$	—	$81 \pm 4$	1	$0.23 \pm 0.01$	—	$0.23 \pm 0.01$	$1.087 \pm 0.009$	$25.74 \pm 1.29$	116/21
		$\pi^+$	$81 \pm 4$	—	$81 \pm 4$	1	$0.33 \pm 0.01$	—	$0.23 \pm 0.01$	$1.087 \pm 0.010$	$25.77 \pm 1.29$	145/21
STAR	200	$\pi^-$	$80 \pm 4$	$169 \pm 10$	$81 \pm 4$	$0.99 \pm 0.01$	$0.22 \pm 0.01$	$0.35 \pm 0.02$	$0.22 \pm 0.01$	$1.048 \pm 0.008$	$0.27 \pm 0.01$	100/6
		$\pi^+$	$80 \pm 4$	$171 \pm 10$	$81 \pm 4$	$0.99 \pm 0.01$	$0.22 \pm 0.01$	$0.35 \pm 0.02$	$0.22 \pm 0.01$	$1.048 \pm 0.008$	$0.28 \pm 0.01$	60/6
ALICE	900	$\pi^-$	$82 \pm 4$	$241 \pm 12$	$83 \pm 4$	$0.99 \pm 0.01$	$0.30 \pm 0.02$	$0.21 \pm 0.01$	$0.30 \pm 0.02$	$1.019 \pm 0.002$	$1.51 \pm 0.08$	172/27
		$\pi^+$	$82 \pm 4$	$241 \pm 12$	$83 \pm 4$	$0.99 \pm 0.01$	$0.30 \pm 0.02$	$0.21 \pm 0.01$	$0.30 \pm 0.02$	$1.019 \pm 0.002$	$1.50 \pm 0.08$	139/27
CMS	900	$\pi^-$	$81 \pm 4$	$241 \pm 12$	$83 \pm 4$	$0.99 \pm 0.01$	$0.30 \pm 0.02$	$0.10 \pm 0.01$	$0.30 \pm 0.01$	$1.004 \pm 0.001$	$3.77 \pm 0.19$	44/16
		$\pi^+$	$81 \pm 4$	$241 \pm 12$	$83 \pm 4$	$0.99 \pm 0.01$	$0.30 \pm 0.02$	$0.10 \pm 0.01$	$0.30 \pm 0.01$	$1.004 \pm 0.001$	$3.78 \pm 0.19$	90/16
	2760	$\pi^-$	$84 \pm 4$	$259 \pm 13$	$86 \pm 4$	$0.99 \pm 0.01$	$0.33 \pm 0.02$	$0.12 \pm 0.01$	$0.32 \pm 0.02$	$1.005 \pm 0.002$	$4.60 \pm 0.23$	29/16
		$\pi^+$	$84 \pm 4$	$260 \pm 13$	$86 \pm 4$	$0.99 \pm 0.01$	$0.33 \pm 0.02$	$0.15 \pm 0.01$	$0.32 \pm 0.02$	$1.005 \pm 0.002$	$4.63 \pm 0.23$	24/16
	7000	$\pi^-$	$86 \pm 4$	$263 \pm 13$	$88 \pm 4$	$0.99 \pm 0.01$	$0.34 \pm 0.02$	$0.18 \pm 0.01$	$0.34 \pm 0.02$	$1.005 \pm 0.003$	$5.83 \pm 0.29$	103/16
		$\pi^+$	$86 \pm 4$	$263 \pm 13$	$88 \pm 4$	$0.99 \pm 0.01$	$0.34 \pm 0.02$	$0.18 \pm 0.01$	$0.34 \pm 0.02$	$1.005 \pm 0.002$	$5.82 \pm 0.29$	89/16
	1300	$\pi^-$	$88 \pm 4$	$278 \pm 14$	$90 \pm 5$	$0.99 \pm 0.01$	$0.36 \pm 0.02$	$0.19 \pm 0.01$	$0.36 \pm 0.02$	$1.005 \pm 0.002$	$5.20 \pm 0.26$	17/16
		$\pi^+$	$88 \pm 4$	$278 \pm 14$	$90 \pm 5$	$0.99 \pm 0.01$	$0.36 \pm 0.02$	$0.19 \pm 0.01$	$0.36 \pm 0.02$	$1.005 \pm 0.002$	$5.37 \pm 0.27$	52/16



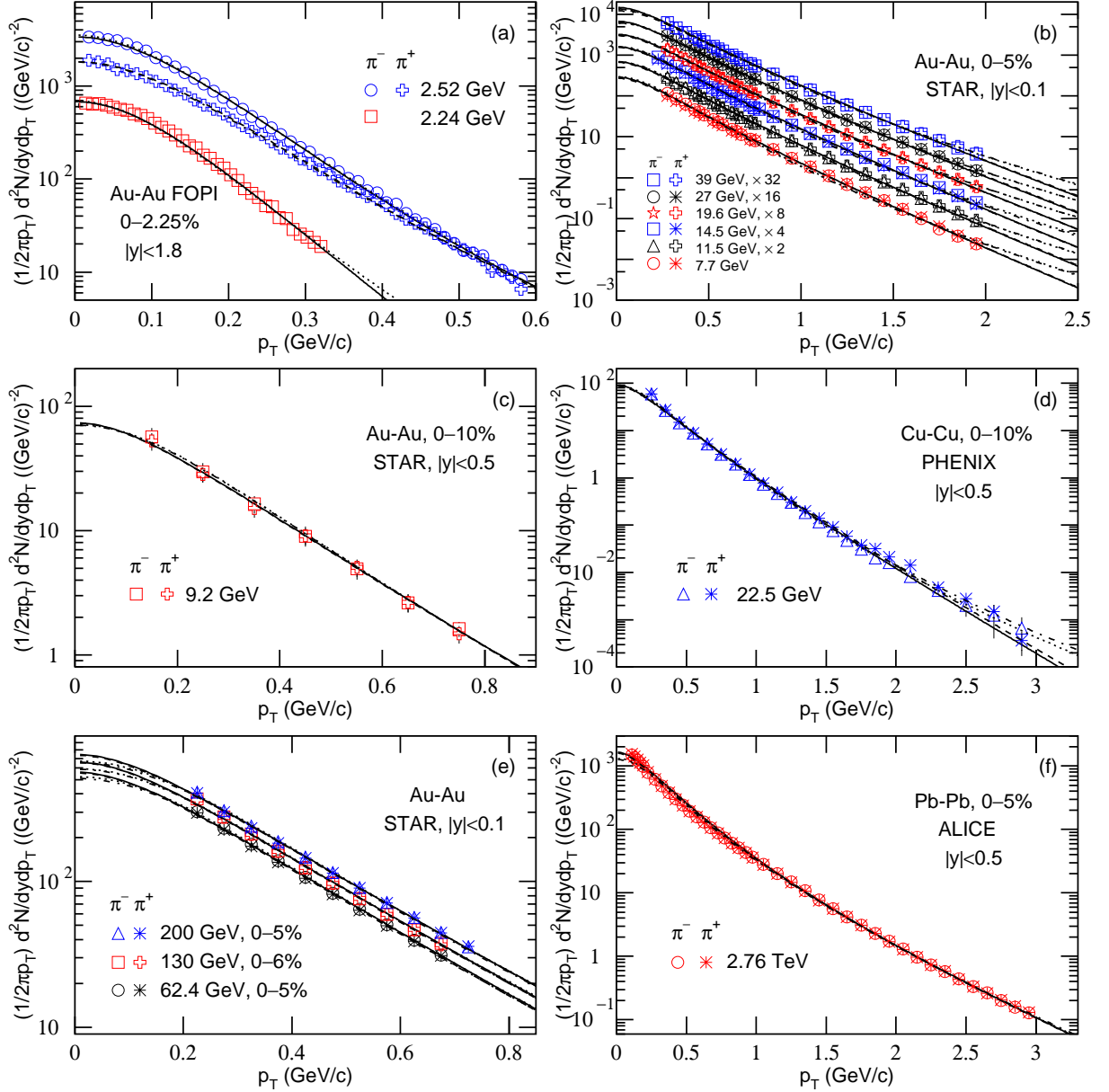


Fig. 2. Same as Fig. 1, but showing the results in central Au-Au (Cu-Cu, Pb-Pb) collisions at high energies. Panels (a)–(f) represent the data measured by the FOPI [22], STAR [27], STAR [28], PHENIX [25], STAR [26], and ALICE [30] Collaborations, respectively, by various symbols. The solid (dashed) curves are our results calculated by Eqs. (1) and (3) for  $\pi^-$  ( $\pi^+$ ) (case III), and the dotted (dotted-dashed) curves are our results calculated by Eqs. (2) and (3) for  $\pi^-$  ( $\pi^+$ ) (case IV). Continuous panels (a)–(f) and (a')–(f') are for ratios of the data to fit obtained from Eqs. (1) and (3) for the case III and from Eqs. (2) and (3) for the case IV respectively.

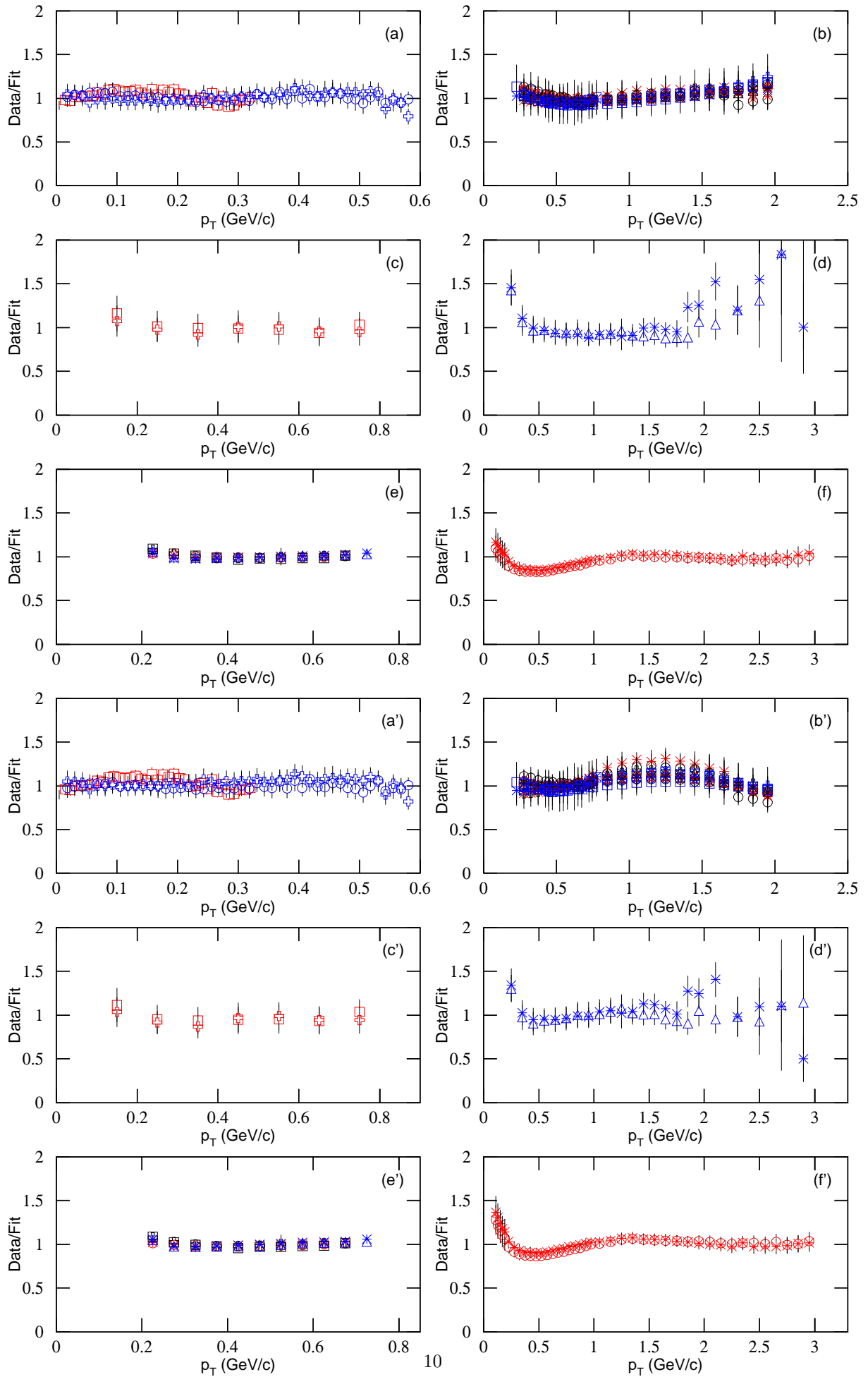


Fig. 2. Continuous.

Table 3. Same as Table 1, but for the solid and dashed curves in Fig. 2 in which the results at mid-rapidity in central nucleus-nucleus collisions are presented.

Collab. and Type	$\sqrt{s_{NN}}$ (GeV)	Particle	$T_1$ (MeV)	$T_2$ (MeV)	$T$ (MeV)	$k$	$\beta_{T_1}$ (c)	$\beta_{T_2}$ (c)	$\beta_T$ (c)	$N_0$	$\chi^2/\text{dof}$
FOPI Au-Au 0-2.25%	2.24	$\pi^-$	$44 \pm 2$	—	$44 \pm 2$	1	$0.28 \pm 0.01$	—	$0.28 \pm 0.01$	$1734.5 \pm 86.7$	29/33
		$\pi^-$	$53 \pm 3$	$98 \pm 5$	$53 \pm 3$	$0.99 \pm 0.01$	$0.22 \pm 0.01$	$0.34 \pm 0.02$	$0.22 \pm 0.01$	$2166.9 \pm 108.3$	7/43
		$\pi^+$	$59 \pm 3$	$98 \pm 5$	$60 \pm 3$	$0.98 \pm 0.01$	$0.22 \pm 0.01$	$0.46 \pm 0.02$	$0.22 \pm 0.01$	$1385.4 \pm 69.3$	12/43
STAR Au-Au 0-5%	7.7	$\pi^-$	$124 \pm 6$	—	$124 \pm 6$	1	$0.40 \pm 0.02$	—	$0.40 \pm 0.02$	$19.8 \pm 1.0$	13/23
		$\pi^+$	$125 \pm 6$	—	$125 \pm 6$	1	$0.40 \pm 0.02$	—	$0.40 \pm 0.02$	$19.0 \pm 1.0$	19/23
0-10%	9.2	$\pi^-$	$117 \pm 6$	—	$117 \pm 6$	1	$0.37 \pm 0.02$	—	$0.37 \pm 0.02$	$21.9 \pm 1.1$	1/4
		$\pi^+$	$117 \pm 6$	—	$117 \pm 6$	1	$0.37 \pm 0.02$	—	$0.37 \pm 0.02$	$21.7 \pm 1.1$	1/4
0-5%	11.5	$\pi^-$	$127 \pm 6$	—	$127 \pm 6$	1	$0.41 \pm 0.02$	—	$0.41 \pm 0.02$	$25.0 \pm 1.3$	10/23
		$\pi^+$	$128 \pm 6$	—	$128 \pm 6$	1	$0.41 \pm 0.02$	—	$0.41 \pm 0.02$	$24.4 \pm 1.2$	15/23
	14.5	$\pi^-$	$129 \pm 6$	—	$129 \pm 6$	1	$0.42 \pm 0.02$	—	$0.42 \pm 0.02$	$29.6 \pm 1.5$	3/25
		$\pi^+$	$129 \pm 6$	—	$129 \pm 6$	1	$0.42 \pm 0.02$	—	$0.42 \pm 0.02$	$29.0 \pm 1.4$	1/25
	19.6	$\pi^-$	$131 \pm 7$	—	$131 \pm 7$	1	$0.43 \pm 0.02$	—	$0.43 \pm 0.02$	$31.1 \pm 1.6$	11/23
		$\pi^+$	$132 \pm 7$	—	$132 \pm 7$	1	$0.43 \pm 0.02$	—	$0.43 \pm 0.02$	$29.8 \pm 1.5$	9/23
	27	$\pi^-$	$132 \pm 7$	—	$132 \pm 7$	1	$0.44 \pm 0.02$	—	$0.44 \pm 0.02$	$33.3 \pm 1.7$	14/23
		$\pi^+$	$133 \pm 7$	—	$133 \pm 7$	1	$0.44 \pm 0.02$	—	$0.44 \pm 0.02$	$33.3 \pm 1.7$	8/23
	39	$\pi^-$	$131 \pm 7$	—	$131 \pm 7$	1	$0.45 \pm 0.02$	—	$0.45 \pm 0.02$	$37.1 \pm 1.9$	23/23
		$\pi^+$	$135 \pm 7$	—	$135 \pm 7$	1	$0.45 \pm 0.02$	—	$0.45 \pm 0.02$	$35.1 \pm 1.7$	15/23
	62.4	$\pi^-$	$134 \pm 7$	—	$134 \pm 7$	1	$0.43 \pm 0.02$	—	$0.43 \pm 0.02$	$41.3 \pm 2.1$	7/4
		$\pi^+$	$133 \pm 7$	—	$133 \pm 7$	1	$0.42 \pm 0.02$	—	$0.42 \pm 0.02$	$41.5 \pm 2.1$	5/4
0-6%	130	$\pi^-$	$134 \pm 7$	—	$134 \pm 7$	1	$0.44 \pm 0.02$	—	$0.44 \pm 0.02$	$50.0 \pm 2.5$	35/4
		$\pi^+$	$134 \pm 7$	—	$134 \pm 7$	1	$0.44 \pm 0.02$	—	$0.44 \pm 0.02$	$49.5 \pm 2.5$	20/4
0-5%	200	$\pi^-$	$136 \pm 7$	—	$136 \pm 7$	1	$0.45 \pm 0.02$	—	$0.45 \pm 0.02$	$57.7 \pm 2.9$	8/5
		$\pi^+$	$136 \pm 7$	—	$136 \pm 7$	1	$0.45 \pm 0.02$	—	$0.45 \pm 0.02$	$57.2 \pm 2.9$	13/5
PHENIX Cu-Cu 0-10%	22.5	$\pi^-$	$131 \pm 7$	—	$131 \pm 7$	1	$0.43 \pm 0.02$	—	$0.43 \pm 0.02$	$35.1 \pm 1.8$	16/20
		$\pi^+$	$133 \pm 7$	—	$133 \pm 7$	1	$0.44 \pm 0.02$	—	$0.44 \pm 0.02$	$34.9 \pm 1.7$	23/20
ALICE	2760	$\pi^-$	$129 \pm 6$	$214 \pm 11$	$139 \pm 6$	$0.89 \pm 0.03$	$0.42 \pm 0.02$	$0.49 \pm 0.03$	$0.44 \pm 0.02$	$810.1 \pm 40.5$	130/35
Pb-Pb 0-5%		$\pi^+$	$129 \pm 6$	$215 \pm 14$	$139 \pm 6$	$0.89 \pm 0.02$	$0.42 \pm 0.02$	$0.49 \pm 0.03$	$0.44 \pm 0.02$	$783.1 \pm 39.2$	85/35

Table 4. Same as Table 1, but one more parameter ( $q$ ) is added and the values correspond to the dotted and dotted-dashed curves in Fig. 2 in which the results at mid-rapidity in central nucleus-nucleus collisions are presented.

Collab. and Type	$\sqrt{s_{NN}}$ (GeV)	Particle	$T_1$ (MeV)	$T_2$ (MeV)	$T$ (MeV)	$k$	$\beta_{T_1}$ (c)	$\beta_{T_2}$ (c)	$\beta_T$ (c)	$q$	$N_0$	$\chi^2/\text{dof}$	
FOPI Au-Au 0-2.25%	2.24	$\pi^-$	$27 \pm 1$	—	$27 \pm 1$	1	$0.16 \pm 0.01$	—	$0.16 \pm 0.01$	$1.073 \pm 0.054$	$1734.5 \pm 86.7$	45/33	
	2.52	$\pi^-$	$32 \pm 2$	—	$32 \pm 2$	1	$0.17 \pm 0.01$	—	$0.17 \pm 0.01$	$1.076 \pm 0.054$	$2205.4 \pm 110.2$	4/43	
		$\pi^+$	$36 \pm 2$	—	$36 \pm 2$	1	$0.18 \pm 0.01$	—	$0.18 \pm 0.01$	$1.079 \pm 0.054$	$1351.5 \pm 67.6$	13/43	
STAR Au-Au	7.7	$\pi^-$	$77 \pm 4$	—	$77 \pm 4$	1	$0.27 \pm 0.01$	—	$0.27 \pm 0.01$	$1.068 \pm 0.053$	$20.2 \pm 1.0$	55/23	
		$\pi^+$	$78 \pm 4$	—	$78 \pm 4$	1	$0.27 \pm 0.01$	—	$0.27 \pm 0.01$	$1.068 \pm 0.053$	$19.2 \pm 0.9$	88/23	
	9.2	$\pi^-$	$77 \pm 4$	—	$77 \pm 4$	1	$0.28 \pm 0.01$	—	$0.28 \pm 0.01$	$1.060 \pm 0.053$	$22.7 \pm 1.1$	1/4	
		$\pi^+$	$77 \pm 4$	—	$77 \pm 4$	1	$0.28 \pm 0.01$	—	$0.28 \pm 0.01$	$1.061 \pm 0.053$	$22.5 \pm 1.1$	2/4	
	11.5	$\pi^-$	$79 \pm 4$	—	$79 \pm 4$	1	$0.29 \pm 0.01$	—	$0.29 \pm 0.01$	$1.068 \pm 0.053$	$25.1 \pm 1.3$	30/23	
		$\pi^+$	$79 \pm 4$	—	$79 \pm 4$	1	$0.29 \pm 0.01$	—	$0.29 \pm 0.01$	$1.068 \pm 0.053$	$25.1 \pm 1.3$	41/23	
	14.5	$\pi^-$	$80 \pm 4$	—	$80 \pm 4$	1	$0.30 \pm 0.01$	—	$0.30 \pm 0.01$	$1.070 \pm 0.054$	$30.5 \pm 1.5$	3/25	
		$\pi^+$	$79 \pm 4$	—	$79 \pm 4$	1	$0.30 \pm 0.01$	—	$0.30 \pm 0.01$	$1.070 \pm 0.054$	$29.5 \pm 1.5$	5/25	
	19.6	$\pi^-$	$82 \pm 4$	—	$82 \pm 4$	1	$0.30 \pm 0.02$	—	$0.30 \pm 0.02$	$1.071 \pm 0.054$	$31.1 \pm 1.6$	12/23	
		$\pi^+$	$82 \pm 4$	—	$82 \pm 4$	1	$0.30 \pm 0.02$	—	$0.30 \pm 0.02$	$1.071 \pm 0.054$	$30.5 \pm 1.5$	17/23	
	27	$\pi^-$	$84 \pm 4$	—	$84 \pm 4$	1	$0.32 \pm 0.02$	—	$0.32 \pm 0.02$	$1.071 \pm 0.054$	$32.8 \pm 1.6$	15/23	
		$\pi^+$	$84 \pm 4$	—	$84 \pm 4$	1	$0.32 \pm 0.02$	—	$0.32 \pm 0.02$	$1.071 \pm 0.054$	$32.8 \pm 1.6$	12/23	
	39	$\pi^-$	$85 \pm 4$	—	$85 \pm 4$	1	$0.32 \pm 0.02$	—	$0.32 \pm 0.02$	$1.071 \pm 0.054$	$36.3 \pm 1.8$	8/23	
		$\pi^+$	$85 \pm 4$	—	$85 \pm 4$	1	$0.33 \pm 0.02$	—	$0.33 \pm 0.02$	$1.072 \pm 0.054$	$34.2 \pm 1.7$	10/23	
	62.4	$\pi^-$	$81 \pm 4$	—	$81 \pm 4$	1	$0.30 \pm 0.02$	—	$0.30 \pm 0.02$	$1.084 \pm 0.054$	$42.7 \pm 2.1$	18/4	
		$\pi^+$	$81 \pm 4$	—	$81 \pm 4$	1	$0.30 \pm 0.02$	—	$0.30 \pm 0.02$	$1.084 \pm 0.054$	$41.5 \pm 2.1$	9/4	
	0-6%	130	$\pi^-$	$82 \pm 4$	—	$82 \pm 4$	1	$0.31 \pm 0.02$	—	$0.31 \pm 0.02$	$1.084 \pm 0.054$	$49.9 \pm 2.5$	42/4
			$\pi^+$	$82 \pm 4$	—	$82 \pm 4$	1	$0.31 \pm 0.02$	—	$0.31 \pm 0.02$	$1.083 \pm 0.054$	$49.1 \pm 2.5$	23/4
	0-5%	200	$\pi^-$	$83 \pm 4$	—	$83 \pm 4$	1	$0.32 \pm 0.02$	—	$0.32 \pm 0.02$	$1.083 \pm 0.054$	$57.7 \pm 2.9$	25/5
			$\pi^+$	$83 \pm 4$	—	$83 \pm 4$	1	$0.32 \pm 0.02$	—	$0.32 \pm 0.02$	$1.083 \pm 0.054$	$56.4 \pm 2.8$	19/5
	PHENIX Cu-Cu 0-10%	22.5	$\pi^-$	$86 \pm 4$	—	$86 \pm 4$	1	$0.32 \pm 0.02$	—	$0.32 \pm 0.02$	$1.059 \pm 0.053$	$36.6 \pm 1.8$	6/20
			$\pi^+$	$86 \pm 4$	—	$86 \pm 4$	1	$0.32 \pm 0.02$	—	$0.32 \pm 0.02$	$1.062 \pm 0.053$	$35.9 \pm 1.8$	19/20
	ALICE Pb-Pb 0-5%	2760	$\pi^-$	$88 \pm 4$	$175 \pm 9$	$94 \pm 5$	$0.93 \pm 0.03$	$0.35 \pm 0.02$	$0.33 \pm 0.03$	$0.35 \pm 0.02$	$1.044 \pm 0.052$	$753.5 \pm 37.7$	64/35
			$\pi^+$	$87 \pm 4$	$175 \pm 9$	$93 \pm 5$	$0.93 \pm 0.02$	$0.35 \pm 0.02$	$0.34 \pm 0.03$	$0.35 \pm 0.02$	$1.044 \pm 0.052$	$722.1 \pm 36.1$	40/35

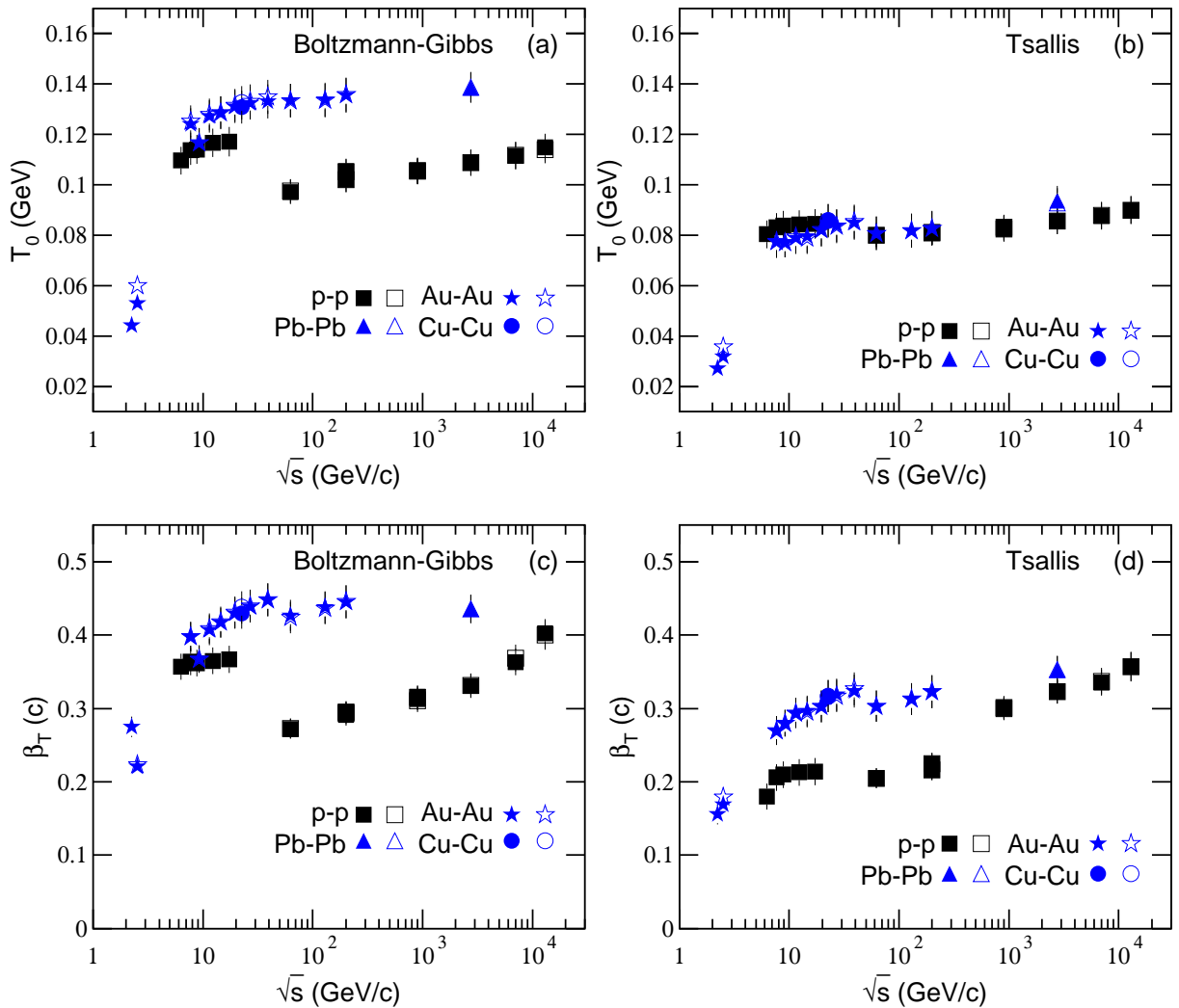


Fig. 3. Energy dependent (a)(b)  $T_0$  and (c)(d)  $\beta_T$  obtained from (a)(c) Eqs. (1) and (3) and from (b)(d) Eqs. (2) and (3). The closed and open symbols represent the parameter values corresponding to  $\pi^-$  and  $\pi^+$  respectively, which are listed in Tables 1–4, where  $\sqrt{s_{NN}}$  for nucleus-nucleus collisions is omitted for concision.

tween the two  $T_0$  render that the chemical freeze-out happens obviously earlier than the kinetic freeze-out due to higher temperature at the chemical freeze-out. The energy deposition in central nucleus-nucleus collisions is larger than that in INEL or NSD  $pp$  collisions due to higher temperature in central nucleus-nucleus collisions. The values of  $T_0$  ( $\beta_T$ ) obtained from Eqs. (2) and (3) are systematically lower than those obtained from Eqs. (1) and (3) by  $\sim 13\%$  ( $\sim 20\%$ ) due to different statistics.

According to an ideal fluid consideration, the time evolution of temperature follows  $T_f = T_i(\tau_i/\tau_f)^{1/3}$ , where  $T_i$  ( $= 300$  MeV) and  $\tau_i$  ( $= 1$  fm) are the initial temperature and proper time respectively [46, 47], and  $T_f$  and  $\tau_f$  denote the final temperature and time respectively. The chemical freeze-out in central nucleus-nucleus collisions happens at about 7.8 fm due to  $T_f = T_{ch} \approx 151$  MeV. The kinetic freeze-out in INEL or NSD

$pp$  collisions happens at 17.8 fm due to  $T_f = T_0 \approx 115$  MeV, and that in central nucleus-nucleus collisions happens at 13.8 fm due to  $T_f = T_0 \approx 125$  MeV, based on Eqs. (1) and (3).

Generally, in low- $p_T$  region,  $T_0$  ( $\beta_T$ ) obtained only from the pion spectra is less than that obtained averagely by weighting the yields of various types of light particles. The treatment in the present work on the extraction of  $T_0$  ( $\beta_T$ ) is approximate. However, the fraction ratio of the pion yield to total yield in high energy collisions is larger ( $\sim 85\%$ ). This approximate treatment is acceptable. The energy dependent  $T_0$  ( $\beta_T$ ) obtained from the pion spectra is similar to that obtained from the weighted average of the spectra of various light particles.

From the RHIC to LHC, there are three trends for the change of  $T_0$ . That is the incremental [14], decreas-

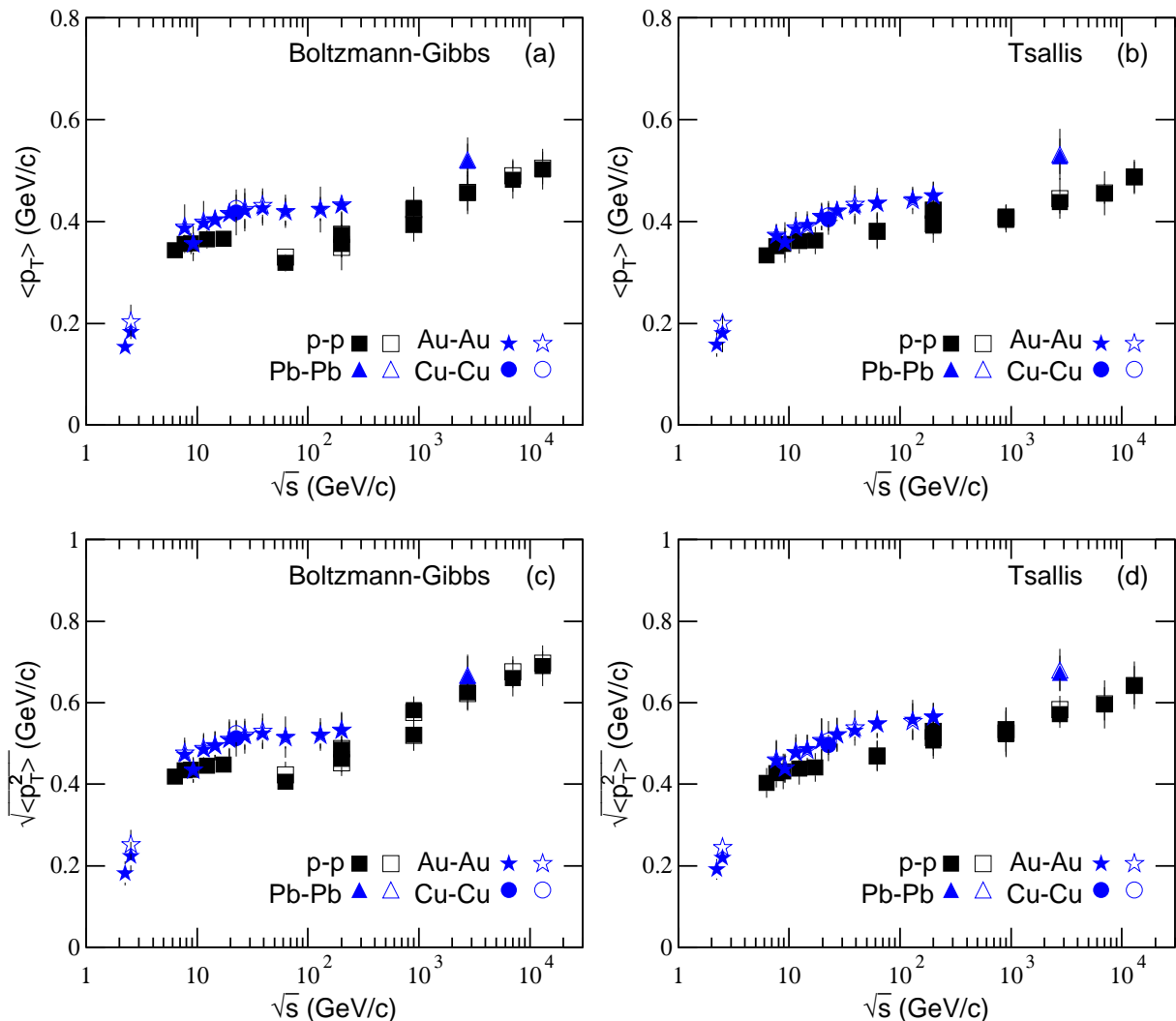


Fig. 4. Energy dependent (a)(b)  $\langle p_T \rangle$  and (c)(d)  $\sqrt{\langle p_T^2 \rangle}$  obtained from (a)(c) Eqs. (1) and (3) and from (b)(d) Eqs. (2) and (3). The closed and open symbols represent the values corresponding to  $\pi^-$  and  $\pi^+$  respectively, where  $\sqrt{s_{NN}}$  for nucleus-nucleus collisions is omitted for concision.

ing [15–20], or invariant trend [12, 13] in the energy dependent  $T_0$ . However, there is only one trend for the change of  $\beta_T$ . That is the incremental trend [12–20] in the energy dependent  $\beta_T$ . The decreasing or invariant trend is not observed in the energy dependent  $\beta_T$ . The present work shows that, in the four cases (two collisions and two statistics), both  $T_0$  and  $\beta_T$  do not decrease from the RHIC to LHC. The energy deposition at the LHC is more than that at the RHIC.

The inconsistent results on the trend of  $T_0$  ( $\beta_T$ ) are in fact caused by different models or methods. Similar to different types of thermometers in thermodynamics, the standard method extracting nuclear temperature is needed in high energy collisions. In our opinion, the standard method should be related to the Boltzmann-Gibbs statistics and the standard distribution (the Boltzmann, Fermi-Dirac, and Bose-Einstein

distributions) which are the foundation of the ideal gas model in thermodynamics. The blast-wave model with Boltzmann-Gibbs statistics [2, 3] and the alternative method [5–11] with standard distribution are suitable to be candidates, though other models and methods also fit the data very well.

In the above discussions, we have used the two-component blast-wave model in some cases. In our very recent work [48], a superposition of the blast-wave model and an inverse power-law has been particularly used in these cases in  $pp$  collisions. It is noted that  $T_0$  ( $\beta_T$ ) is mainly determined by the first component due to the fact that the first component contributes a major fraction. From the point of view of extraction of  $T_0$  ( $\beta_T$ ), one can consider only the contribution of the first component. Even the second component can be given up in the fit process and the corresponding  $p_T$  region can be

left there.

In the last part of this section, we would like to discuss further some issues. The description of blast-wave model came from Ref. [2] assumes the local thermal equilibrium based on a hydrodynamical framework. From Cooper-Frye formula, one can derive Eq. (1) for Boltzmann-Gibbs statistics. Due to the very short interacting time, the collision system is possibly not in the thermal equilibrium with an unified temperature, but in a few local thermal equilibriums with different temperatures. Naturally and in the simplest way, we can use the two-component blast-wave model, which basically assumes that the both very-low- $p_T$  and low- $p_T$  particles severally obey the above hydrodynamical assumption.

Although the system of  $pp$  collisions at low energy is probably not in thermal equilibrium or local thermal equilibriums due to low multiplicity, the present work treats  $pp$  collisions at high energies in which the multiplicities in most cases are not too low. In particular, small collision systems such as  $pp$  and  $p$ -nucleus collisions show abundant collective behaviors [49] which are similar to those in nucleus-nucleus collisions. These similarities to nucleus-nucleus collisions render that the idea of local thermal equilibrium for  $pp$  collisions at high energies may be the truth. The application of the (two-component) blast-wave model in  $pp$  collisions at high energies is acceptable.

In addition, we would like to emphasize that, comparing with central nucleus-nucleus collisions or with the blast-wave model with Tsallis statistics, we have observed the inconsistent trend for the energy dependence of  $T_0$  ( $\beta_T$ ), i.e. the hill, in  $pp$  collisions analyzed by the blast-wave model with Boltzmann-Gibbs statistics. This implies that the successional or cascade nucleon-nucleon collisions and multiple scattering of secondary particles in central nucleus-nucleus collisions play important roles in the collision process. Due to these successional collisions and multiple scattering, some statistical and/or dynamical fluctuations in  $pp$  collisions are smoothed obviously in central nucleus-nucleus collisions. In the blast-wave model with Tsallis statistics, the extra entropy index  $q$  smoothes naturally these fluctuations.

## 4 Conclusions

To conclude, the transverse momentum spectra of  $\pi^-$  and  $\pi^+$  produced at mid-(pseudo)rapidity in INEL or NSD  $pp$  collisions and in central Au-Au (Cu-Cu, Pb-Pb) collisions over an energy range from the SIS to LHC have been analyzed by the (two-component) blast-wave model with Boltzmann-Gibbs statistics and with Tsallis statistics. The model results are in similarly well agreement with the experimental data of FOPI, NA61/SHINE, STAR, PHENIX, ALICE, and CMS Col-

laborations. The values of related parameters, the kinetic freeze-out temperature  $T_0$  and the transverse flow velocity  $\beta_T$ , are extracted from the fit process and the energy dependent parameters are obtained.

In INEL or NSD  $pp$  collisions and analyzed by the blast-wave model with Boltzmann-Gibbs statistics, both the energy dependent  $T_0$  and  $\beta_T$  show complex structure. There is a hill at  $\sqrt{s} \approx 10$  GeV, a drop at dozens of GeV, and an increase from dozens of GeV to above 10 TeV. In central Au-Au (Cu-Cu, Pb-Pb) collisions or analyzed by the blast-wave model with Tsallis statistics, both the energy dependent  $T_0$  and  $\beta_T$  show simple structure. Form the SIS to LHC, there is a quick increase before 10 GeV, and then a slight increase or saturation after 10 GeV. The differences among the energy dependent parameters in different cases are caused by different collision systems and statistics. Large system smoothes the fluctuations due to the successional collisions and multiple scattering. The Tsallis statistics smoothes the fluctuations due to the entropy index.

Some special properties result in the special energy of 10 GeV (11 GeV more specifically [45]). At this special energy, not only the final state has the highest net baryon density, but also the transition from a baryon-dominated to a meson-dominated final state had happened. At the same time, the ratios of strange particles to mesons show clear and pronounced maximums at this energy. Regardless of the baryon-dominated and meson-dominated final state, they are possible to undergo a parton-dominated intermediate state at higher energy. To search for the critical energy at which the parton-dominated intermediate state appears initially is a long-term target, though the critical energy is possibly around the energy bridge from the SPS to RHIC.

### Data Availability

All data are quoted from the mentioned references. As a phenomenological work, this paper does not report new data.

### Conflicts of Interest

The authors declare that there are no conflicts of interest regarding the publication of this paper.

### Acknowledgments

This work was supported by the National Natural Science Foundation of China under Grant Nos. 11575103 and 11747319, the Shanxi Provincial Natural Science Foundation under Grant No. 201701D121005, and the Fund for Shanxi “1331 Project” Key Subjects Construction.

## References

- [1] A. Puglisi, A. Sarracino, A. Vulpiani, Phys. Rep. **709**, 1 (2017).

- [2] E. Schnedermann, J. Sollfrank, U. Heinz, Phys. Rev. C **48**, 2462 (1993)
- [3] STAR Collaboration (B.I. Abelev *et al.*), Phys. Rev. C **81**, 024911 (2010).
- [4] Z.B. Tang, Y.C. Xu, L.J. Ruan, G. van Buren, F.Q. Wang, Z.B. Xu, Phys. Rev. C **79**, 051901(R) (2009).
- [5] Z.B. Tang, L. Yi, L.J. Ruan, M. Shao, H.F. Chen, C. Li, B. Mohanty, P. Sorensen, A.H. Tang, Z.B. Xu, Chin. Phys. Lett. **30**, 031201 (2013).
- [6] K. Jiang, Y.Y. Zhu, W.T. Liu, H.F. Chen, C. Li, L.J. Ruan, Z.B. Tang, Z.B. Xu, Phys. Rev. C **91**, 024910 (2015).
- [7] H. Heiselberg, A.M. Levy, Phys. Rev. C **59**, 2716 (1999).
- [8] S. Takeuchi, K. Murase, T. Hirano, P. Huovinen, Y. Nara, Phys. Rev. C **92**, 044907 (2015).
- [9] H.-R. Wei, F.-H. Liu, R.A. Lacey, Eur. Phys. J. A **52**, 102 (2016).
- [10] H.-R. Wei, F.-H. Liu, R.A. Lacey, J. Phys. G **43**, 125102 (2016).
- [11] H.-L. Lao, H.-R. Wei, F.-H. Liu, R.A. Lacey, Eur. Phys. J. A **52**, 203 (2016).
- [12] A. Andronic, Int. J. Mod. Phys. A **29**, 1430047 (2014).
- [13] ALICE Collaboration (B. Abelev *et al.*), Phys. Rev. Lett. **109**, 252301 (2012).
- [14] S. Zhang, Y.G. Ma, J.H. Chen, C. Zhong, Adv. High Energy Phys. **2015**, 460590 (2015).
- [15] S. Das for the STAR collaboration, EPJ Web of Conf. **90**, 08007 (2015).
- [16] S. Das for the STAR collaboration, Nucl. Phys. A **904–905**, 891c (2013).
- [17] S. Zhang, Y.G. Ma, J.H. Chen, C. Zhong, Adv. High Energy Phys. **2016**, 9414239 (2016).
- [18] STAR Collaboration (L. Adamczyk *et al.*), Phys. Rev. C **96**, 044904 (2017).
- [19] X.F. Luo, Nucl. Phys. A **956**, 75 (2016).
- [20] S. Chatterjee, S. Das, L. Kumar, D. Mishra, B. Mohanty, R. Sahoo, N. Sharma, Adv. High Energy Phys. **2015**, 349013 (2015).
- [21] H.-L. Lao, F.-H. Liu, B.-C. Li, M.-Y. Duan, Nucl. Sci. Tech. **29**, 82 (2018).
- [22] FOPI Collaboration (W. Reisdorf *et al.*), Nucl. Phys. A **781** 459 (2007).
- [23] NA61/SHINE Collaboration (N. Abgrall *et al.*), Eur. Phys. J. C **74**, 2794 (2014).
- [24] PHENIX Collaboration (A. Adare *et al.*), Phys. Rev. C **83**, 064903 (2011).
- [25] J.T. Mitchell for the PHENIX Collaboration, PoS(CPOD2006)019, arXiv:nucl-ex/0701079.
- [26] STAR Collaboration (B.I. Abelev *et al.*), Phys. Rev. C **79**, 034909 (2009).
- [27] STAR Collaboration (L. Adamczyk *et al.*), Phys. Rev. C **96**, 044904 (2017).
- [28] STAR Collaboration (B.I. Abelev *et al.*), Phys. Rev. C **81**, 024911 (2010).
- [29] ALICE Collaboration (K. Aamodt *et al.*), Eur. Phys. J. C **71**, 1655 (2011).
- [30] ALICE Collaboration (B. Abelev *et al.*), Phys. Rev. Lett. **109**, 252301 (2012).
- [31] CMS Collaboration (S. Chatrchyan *et al.*), Eur. Phys. J. C **72**, 2164 (2012).
- [32] CMS Collaboration (A.M. Sirunyan *et al.*), Phys. Rev. D **96**, 112003 (2017).
- [33] R. Odorico, Phys. Lett. B **118**, 151 (1982).
- [34] UA1 Collaboration (G. Arnison *et al.*), Phys. Lett. B **118**, 167 (1982).
- [35] T. Mizoguchi, M. Biyajima, N. Suzuki, Int. J. Mod. Phys. A **32**, 1750057 (2017).
- [36] R. Hagedorn, Riv. Nuovo Cimento **6**(10), 1 (1983).
- [37] ALICE Collaboration (B. Abelev *et al.*), Eur. Phys. J. C **75**, 1 (2015).
- [38] ALICE Collaboration (K. Aamodt *et al.*), Phys. Lett. B **693**, 53 (2010).
- [39] A. De Falco for the ALICE collaboration, J. Phys. G **38**, 124083 (2011).
- [40] ALICE Collaboration (B. Abelev *et al.*), Phys. Lett. B **710**, 557 (2012).
- [41] HERA-B Collaboration (I. Abt *et al.*), Eur. Phys. J. C **50**, 315 (2007).
- [42] ALICE Collaboration (B. Abelev *et al.*), Phys. Lett. B **718**, 295 (2012) and Erratum: Phys. Lett. B **748**, 472 (2015).
- [43] I. Lakomov for the ALICE collaboration, Nucl. Phys. A **931**, 1179 (2014).
- [44] ALICE Collaboration (B. Abelev *et al.*), Phys. Lett. B **708**, 265 (2012).
- [45] J. Cleymans, arXiv:1711.02882 [hep-ph] (2017).
- [46] J.D. Bjorken, Phys. Rev. D **27**, 140 (1983).
- [47] K. Okamoto, C. Nonaka, Eur. Phys. J. C **77**, 383 (2017).
- [48] L.-L. Li, F.-H. Liu, arXiv:1805.03342 [hep-ph] (2018).
- [49] H.C. Song, Y. Zhou, K. Gajdošová, Nucl. Sci. Tech. **28**, 99 (2017).